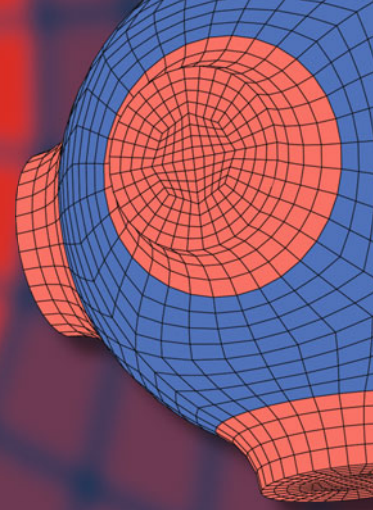Alexander D. Pogrebnjak
Yang Bing
Martin Sahul   *Editors*

Nanocomposite and Nanocrystalline Materials and Coatings

Microstructure, Properties and Applications

Springer

Advanced Structured Materials

Volume 214

Series Editors

Andreas Öchsner, Faculty of Mechanical and Systems Engineering, Esslingen
University of Applied Sciences, Esslingen, Germany

Lucas F. M. da Silva, Department of Mechanical Engineering, Faculty of
Engineering, University of Porto, Porto, Portugal

Holm Altenbach , Faculty of Mechanical Engineering, Otto von Guericke
University Magdeburg, Magdeburg, Sachsen-Anhalt, Germany

Common engineering materials are reaching their limits in many applications, and new developments are required to meet the increasing demands on engineering materials. The performance of materials can be improved by combining different materials to achieve better properties than with a single constituent, or by shaping the material or constituents into a specific structure. The interaction between material and structure can occur at different length scales, such as the micro, meso, or macro scale, and offers potential applications in very different fields.

This book series addresses the fundamental relationships between materials and their structure on overall properties (e.g., mechanical, thermal, chemical, electrical, or magnetic properties, etc.). Experimental data and procedures are presented, as well as methods for modeling structures and materials using numerical and analytical approaches. In addition, the series shows how these materials engineering and design processes are implemented and how new technologies can be used to optimize materials and processes.

Advanced Structured Materials is indexed in Google Scholar and Scopus.

Alexander D. Pogrebnjak · Yang Bing ·
Martin Sahul

Editors

Nanocomposite and Nanocrystalline Materials and Coatings

Microstructure, Properties and Applications

Springer

Editors
Alexander D. Pogrebnjak
Department of Nanoelectronics
Sumy State University
Sumy, Ukraine

Yang Bing
School of Power and Mechanical
Engineering
Wuhan University
Wuhan, Hubei, China

Martin Sahul
Institute of Materials Science
Slovak University of Technology
Trnava, Slovakia

Paper in this product is recyclable.

Preface

In contemporary industries, the widespread utilization of nanocomposites and other nanomaterials is evident. Notably, these materials have emerged as protective coatings and films, enhancing the performance characteristics of cutting tools, stamps, and various components susceptible to wear. Consequently, this field of solid-state physics and materials science holds considerable appeal for a diverse audience of researchers. Engaging scientists and engineers, it also captivates the interest of Ph.D. and master students in related specialties, such as micro- and nanoelectronics. This book encompasses a collection of chapters that meticulously outline the current state of various research areas. It explores topics such as diborides, their intricate structure, properties, and promising applications, the book delves into the forefront of materials science. Additionally, it delves into the highly sought-after topic of nitrides based on high-entropy alloys, dissecting their properties and structure. Furthermore, the book navigates the cutting-edge advancements in antiferromagnetic spintronic oscillators and sheds light on Terahertz signal detectors based on antiferromagnetic spintronic nanostructures. A series of original chapters dedicated to the deposition and exploration of protective coatings tailored for diverse applications are also included. Through these comprehensive explorations, this book can provide valuable insights for researchers, scholars, and students working in the ever-evolving field of materials science.

Sumy, Ukraine/Trnava, Slovak Republic   Alexander D. Pogrebnjak
Wuhan, China   Yang Bing
Trnava, Slovak Republic   Martin Sahul

Contents

Hard Transition-Metal Diboride Coatings

Check for updates

Marián Mikula

Abstract Transition-metal diborides (TMB$_2$, TM = Ti, Zr, Hf, V, Nb, Ta, Co, Mo, and W) form extremely temperature-stable single-phase compositions belonging to ultra-high temperature ceramics. The strong ionic and covalent bonds between atoms of transition metal and boron atoms in the hexagonal a-AlB$_2$ or w-W$_2$B$_5$ type of TMB$_2$ structure led to the high hardness, excellent wear resistance, and chemical inertness of these materials. Physical deposition methods enhance TMB$_2$'s intrinsic character by forming hard coatings. Hard TMB$_2$ coatings typically have a nanocomposite structure consisting of nanocolumns with a diameter of a few nanometers and an amorphous, so-called B-tissue phase. These coatings are very hard, often more than 40 GPa. However, TMB$_2$ coatings still do not fulfill their application potential in demanding thermal–mechanical conditions due to their low oxidation resistance compared to the bulk equivalent, inherent brittleness, and poor crack propagation resistance. This chapter demonstrates a variety of approaches to tuning the mechanical properties and improving the weaknesses of these promising materials using both deposition methods (changing deposition parameters and ionizing sputtered species) and material design (changing stoichiometry, alloying, and multilayer architecture).

Keywords Transition-metal diborides · Hard coatings · Magnetron sputtering · Nanostructure · Mechanical properties · Alloying · Multilayers

M. Mikula (✉)
Fakulty of Mathematics, Physics, and Informatics, Comenius University in Bratislava, Mlynská Dolina F2, Bratislava, Slovak Republic
e-mail: marian.mikula@fmph.uniba.sk

Institute of Materials and Machine Mechanics, Slovak Academy of Sciences, Dúbravská Cesta 9/6319, Bratislava, Slovak Republic

1 Introduction

In general, hard coatings represent a group of materials that are attractive due to their mechanical properties, especially their high hardness and good resistance to abrasive and erosive wear, but also their low coefficient of friction under certain environmental conditions. These properties are also accompanied by excellent oxidation and corrosion resistance at elevated temperatures. Hard coatings, usually a few micrometers thick, have found their application on cutting plates of machining tools, on forming and casting molds, or on components (engine blocks, nozzles, turbine blades, etc.) in the automotive and aviation industries. In addition, hard coatings also serve as diffusion barriers in microelectronics or as decorative coatings.

Hard coatings based on transition-metal nitrides (TMN) have dominated the deposition industry for decades, where physical deposition techniques (PVD), especially ARC evaporation or magnetron sputtering, are used in their preparation.

The structure of TMN coatings is most often face-centered cubic single-phase (TiN, CrN) [1–4] or formed by a metastable multi-element solid solution (TiAlN, CrAlN, TaAlN, TiAlTaN) [5–14], which tends to spinodally decompose at high temperatures (700–1000 °C) into a stable multiphase structure. These decomposition processes are often accompanied by an increase in hardness—the so-called age hardening.

Another group of materials to which this chapter is devoted are transition-metal diborides (TMB$_2$), representing a promising alternative to hard TMN coatings in demanding high-temperature applications. In general, the combination of boron and metals represents a large family of materials with different crystallographic structures and physical properties, from hard orthorhombic monoborides (TiB, CrB, FeB) [15–18], through superconducting hexagonal MgB$_2$ [19], hard and superconducting tetragonal Mo$_2$B [20], tetragonal magnetic ReB$_4$ [21], hexagonal LaB$_6$ used in hot cathodes [22], to very hard and low-friction orthorhombic ternary so-called BAM systems with AlMgB$_{14}$ composition [23].

The hard coatings described here are based on diborides of IVB–VIB transition metals belonging to the group of so-called ultra-high temperature ceramics (UHTC). These materials crystallize in the hexagonal a-AlB$_2$ or w-W$_2$B$_{5-x}$-type of structure, where the atoms are bonded by strong covalent and ionic bonds, which leads to high-temperature chemical stability and excellent mechanical properties [24]. Unlike TM nitride coatings, TM-diboride coatings prepared by PVD methods usually have a nanocomposite character formed by TMB$_2$ nanocolumns surrounded by amorphous boron, the so-called B-tissue phase, and such a structure shows an extremely high hardness >40 GPa [25]. Unfortunately, the presence of the B-tissue phase causes significantly lower oxidation resistance of TMB$_2$ coatings at elevated temperatures compared to their bulk equivalents [26, 27]. In addition, TMB$_2$ coatings have a typical brittle ceramic character and low resistance to crack propagation [28]. These weaknesses significantly limit their application potential, and, although TMB$_2$ coatings achieve higher hardness than TMN coatings, they are currently unable to effectively alternate them.

In the following section, transition-metal diborides are described from the point of view of their basic properties, chemical bonds, band structure, and electronic structure. The influence of deposition effects on the formation of the coating nanostructure, stoichiometry, and their mechanical properties is discussed in the next section. The following is a discussion of the B-tissue phase and methods of its reduction through progressive physical deposition methods. Another section is devoted to the formation of ternary diboride systems with increased temperature stability and improved oxidation resistance. The last section is focused on the fracture behavior of TMB_2 coatings and promising ways to improve the fracture toughness by alloying with ductile metal or through the concept of superlattices and multilayer systems.

2 Transition-Metal Diborides

Diborides of transition metals from groups IVB to VIB of the periodic table are classified as ultra-high-temperature ceramics. In the transition-metal-boron equilibrium binary diagrams, TMB_2 are formed as single-phase compositions in a very narrow concentration ratio, which are characterized by high melting temperature values in the range of ~2200 °C (CrB_2) to 3400 °C (HfB_2). However, some TM diborides from the IIIB (YB_2) and VIIB (ReB_2) groups are also interesting in demanding thermal and mechanical conditions.

In general, TMB_2 crystallize in two different hexagonal structures. So-called early TMB_2 (e.g., TiB_2, ZrB_2, HfB_2, and NbB_2) prefer the α-AlB_2 structure type (space group 191-P6/mmm) where α-structure consists of a hexagonal-shaped unit cell with an alternating stacking of covalently bonded boron hexagons and metal layers. So-called late TMB_2 (e.g., MoB_2, WB_2) form the ω-W_2B_{5-x} (space group 194-P63/mmc) consisting of hexagonal-shaped unit cells with alternating flat and puckered boron hexagons between the metal layers [24], as can be seen in Fig. 1. However, as will be shown in the next chapters, thermodynamically non-equilibrium TMB_2 synthesis processes, e.g., into coatings, led to the formation of the α-AlB_2 structure across the diborides of all transition metals, even in the case of lower chemical stability of the a-structure compared to the w-structure. For this reason, we will demonstrate the electronic nature of bonds and their influence on stability, mechanical properties, and lattice parameters only on the α-AlB_2 type of structure.

A closer description of the α-AlB_2 structure (Fig. 1a) shows that this structure is quite tightly packed. Boron atoms lie on the corners of hexagons, with the three nearest neighboring boron atoms in each plane. The TM atoms lie directly in the center of each boron hexagon but midway between adjacent boron layers; each TM atom has 12 nearest neighboring B atoms and six nearest neighboring atoms in the TM plane. The in-plane distance between adjacent TM–TM atoms is equal to the lattice parameter a. The lattice parameter c represents the distance between the nearest planes occupied by TM atoms (Fig. 1a).
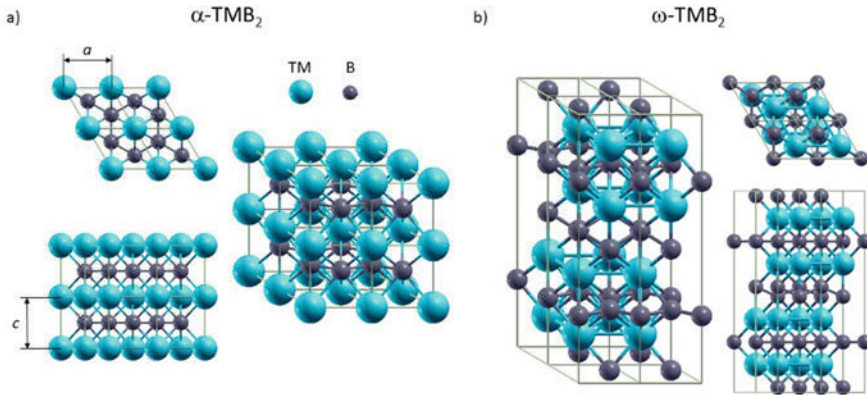
Fig. 1 Illustration of the supercell of **a** the a and **b** the w phases of transition-metal diborides

2.1 Density of States

The total electron density of states (TDOS) histogram provides a qualitative view of the chemical bonds between boron atoms and transition metals. Figure 2 shows the projected densities of states of selected systems representing diborides of elements from the IIIB to VIB groups. The vertical line indicates the Fermi level (E_F). The TDOS histograms of TMB_2 consist of several parts [29]: (a) a region present in the low-energy part of the curve (~ -14 to -8 eV), which is mainly formed by tightly bonded B-2s electrons; these electrons are localized and their effect on bonding is small; (b) a region with a maximum around -5 eV showing, at lower energies, bonding states that are mainly formed by overlapping B sp^2–B sp^2 and B-2p–B-2p orbitals. At higher energies approaching the Fermi level, this region ends with a sharp valley—the so-called pseudogap. To the left of the valley, the density of states is formed by mutual interactions of B-2p–TM-d orbitals as well as interactions of TM-d–TM-d and B-2p–B-2p orbitals [30]; (c) to the right of the valley, there is a peak showing high-energy bonding states on the TDOS curve, which are dominantly formed by the contribution from antibonding TM-d-states. This peak shifts toward lower energies due to an increase in the number of valence electrons from transition metals with three valence electrons (Y), through four valence electrons (Zr, Ti) to the group with five (Nb, Ta), and six valence electrons (Mo, W), respectively. This also changes the nature of interactions between atoms of transition metals and boron when the increasing number of valence electrons strengthens TM–B interactions and weakens TM-d–TM-d interactions.

This is an important fact that significantly determines not only the chemical stability of TM diborides but also their electrical conductivity and mechanical properties. As can be seen in YB_2 (Fig. 2a), the Fermi level is located below the peak of the bonding states, which indicates that the valence bands are partially filled and therefore the chemical stability of YB_2 is lower. In addition, the final states at the
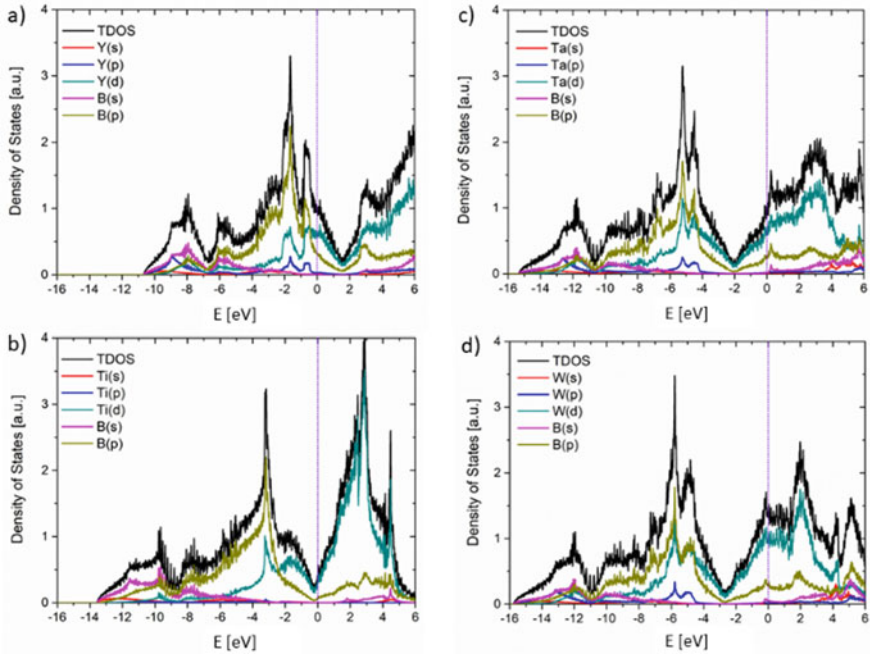
Fig. 2 Total electron density of states for **a** *3d* YB$_2$; **b** *4d* TiB$_2$; **c** *5d* TaB2; **d** *6d* WB$_2$

Fermi level formed by contributions from the Y-4d and B-2p states indicate metallic electrical conductivity in this ceramic material [30, 31].

A higher number of electrons—four in TiB$_2$ (Fig. 2b)—primarily shifts the TDOS to lower energies. At the same time, the Fermi level lies on the pseudogap, which means that the valence bands are fully filled and the chemical stability of TiB$_2$ is significantly higher compared to YB$_2$ (T$_{mTiB2}$ ~ 3220 °C > T$_{mYB2}$ ~ 2100 °C); on the contrary, the electrical conductivity is lower due to the lower number of states near the E$_F$. This situation changes in TaB2 and WB$_2$ with a higher number of valence electrons, where, according to Mott's law [32], the electrical conductivity increases due to the increasing number of states near E$_F$. On the other hand, as can be seen in Fig. 2c and d, if the number of valence electrons is 5 or 6, the Fermi level is above the bottom of the antibonding states that are occupied by the excess electrons. This leads to lower chemical stability and lower melting temperatures of these TMB$_2$ compounds (T$_{mTaB2}$ ~ 3000 °C, T$_{mWB2}$ ~ 2400 °C) compared to TM diborides from the IVB group.

The projected density of states also explains the mechanical behavior of TMB$_2$ from the perspective of chemical bonds. The presence of B2p–TM-d bonds and especially TM-d–TM-d bonds determines the bulk modulus (B) as well as the shear modulus (G) of these ceramic materials. Increasing values of B correlate with an increasing number of valence electrons. The highest bulk moduli have diborides VB and VIB of transition metals, where, unlike diborides IIIB and IVB, the presence of

both B2p–TM-d bonds and TM-d–TM-d bonds contributes to increasing B values [33].

In the case of shear moduli, B2p–TM-d states play an important role, where their gradual filling with an increasing number of valence electrons from three to four leads to an increase in G. However, their subsequent saturation and occupation of antibonding d-states (in the transition metals with five and six valence electrons, respectively) lead to a decrease in shear modulus values [30].

The G/B ratio defined as Pugh's criterion for distinguishing ductile from brittle materials indicates that while TM (IIIB-VB)-B_2 exhibits brittle behavior, TM(VIB)-B_2 behaves ductile during mechanical loading [30].

In addition, the values of B and G determine Young's modulus E of TMB_2 and can also be used in the empirical model of Chen et al. [34] to estimate hardness. Young's modulus follows a similar trend to shear modulus, where TM (IVB-VB)-diborides (TiB_2, ZrB_2, HfB_2, NbB_2, or VB_2) have the highest E values exceeding 500 GPa, leading to poor thermal shock resistance. Conversely, TM (IIIB and VIB)-diborides exhibiting lower E values (YB_2 ~ 342 GPa, MoB_2 ~ 452 GPa, and WB_2 ~ 423 GPa) are more thermally resistant [30]. According to [34] TM diborides such as TiB_2 or ZrB_2 with high E values are extremely hard, with hardness exceeding 40 GPa. The decreasing trend of hardness is correlated with the decrease of Young's modulus, where the hardness of, e.g., TaB2 and WB_2 is 25 GPa and 15 GPa, respectively [30]. It is important to note that the hardness values calculated in this empirical model may not accurately reflect the true hardness of TMB_2. However, as will be shown in the following sections, this prediction of hardness, e.g., in the case of ZrB_2 or TiB_2, is in good agreement with superhard ZrB_2 [35] and TiB_2 [25, 36] coatings; in the case of CrB_2 [37] or WB_2 [38] the predicted hardness is rather close to their sintered bulk forms.

2.2   Charge Density Maps

Charge density maps show charge redistributions due to the formation of chemical bonds between atoms in transition-metal diborides. This can be illustrated for ZrB_2 [39]. Here, the electron charge density in the 0001 plane across the Zr atoms (Fig. 3a) shows the metallic Zr–Zr bonds, as demonstrated by the uniform distribution of the charge density between neighboring Zr atoms. On the contrary, strong electron localization is visible between neighboring B atoms in the graphic-like 0002 plane, and B–B bonds have an s-type covalent character formed by overlapping hybridized B sp^2–B sp^2 orbitals (Fig. 3b). However, strong electron localization is also found between neighboring B atoms in the (11–20) plane, where B–B bonds are p-type covalent in nature and are formed by overlapping $B2p_z$–$B2p_z$ orbitals. The Zr–B bonds shown on the (11–20) plane are ionic-covalent (Fig. 3c); here, the ionic character is given by charge transfer from Zr to B atoms, and lobes formed by weak interactions between Zr $4d(t_{2g})$ and B $2p_z$ orbitals indicate Zr–B covalent bonds.

Fig. 3 Charge density maps for ZrB$_2$ in **a** the (0001) plane where the Zr–Zr bonding is present, **b** the (0002) plane where the B–B bonding is present, and **c** the (10–10) plane where the Zr–Zr, B–B, and Zr–B bondings are present
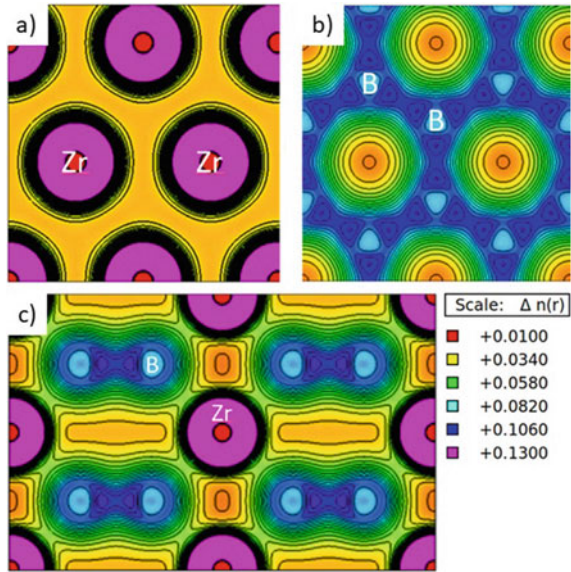
Changes in the lattice parameters are also related to the nature of the chemical bonds between atoms of transition metals and boron. In the hexagonal α-AlB$_2$-type structure, the lattice constant c is larger than a due to the chemical bond anisotropy since the B–B covalent s-type as well as the p-type bonds are stronger than the ionic-covalent TM–B bonds. In addition, both lattice constants a and c, respectively, decrease with increasing numbers of valence electrons in transition metals. This decrease is caused by the strengthening of the bonds by gradually filling the valence bands from partially filled (YB$_2$) to fully filled (ZrB$_2$). In the case of TMB$_2$ with a high number of valence electrons (CrB$_2$, WB$_2$), where the excess electrons fill the antibonding d-states, the decrease in the lattice constant c is due to the enhancement of TM–B bonds by TM d(t$_{2g}$)–B 2p$_z$ and TM d(t$_{2g}$)–B sp^2.

3 Deposition of Transition-Metal Diboride Coatings

Looking at the history of the twentieth century, many technological approaches, based on chemical (CVD) or physical (PVD) vapor deposition, have been developed to prepare TMB$_2$ coatings [40]. CVD methods use toxic borane-based precursors that condense at very high temperatures (>900 °C) for the growth of TiB$_2$ [41, 42] and ZrB$_2$ coatings [43–45]. However, these extreme conditions preclude the use of technical materials, e.g., high-speed steels and alloys, and represent a burden on the environment. From the PVD methods, E-beam vaporization [46], pulsed laser deposition [47, 48], and reactive sputter process [49] proved to be suitable for the growth of very hard, crystalline, highly oriented, or epitaxial TiB$_2$ or ZrB$_2$ films

on monocrystalline substrates such as sapphire, SiC, and silicon. However, again, these depositions are accompanied by high temperatures of 600–900 °C, and, for that reason, these PVD methods are more suitable for basic research on TMB_2 coatings than for producing coatings on an industrial scale.

Logically, one could expect that cathodic arc deposition, dominantly used for the industrial production of hard coatings, could also be suitable for the deposition of TMB_2 coatings. But early research on TiB_2 arc coatings showed problems: stabilizing the arc discharge and generating large amounts of macroparticles due to the high melting temperature of TiB_2 targets [50]. Further modifications of the cathode processes, from alloying the target with a small amount (a few wt.%) of aluminum or carbon [50] through arc pulsing [51] to controlling the movement of the arc-spot by an external magnetic field [52], led to higher stability of the processes and the suppression of macroparticle generation and subsequent growth of hard TiB_2 coatings on externally unheated steel substrates. Despite these positive results, the optimization processes have not yet been completed, and studies of the behavior of other arc TM-diboride cathodes are also lacking. For these reasons, the commercial production of TMB_2 coatings using cathodic arc deposition has not yet started.

Undoubtedly, the most widely used method for preparing TM-diboride coatings in lab-scale or industry-scale equipment, respectively, is direct current (DC) magnetron sputtering. Here, a sintered stoichiometric diboride compound target is sputtered using an inert (argon) glow discharge, and high-quality TMB_2 coatings can be prepared already at low deposition temperatures (on an externally unheated substrate).

However, there are several important aspects that affect the resulting chemical composition, structure, and physical properties of the coatings. The first aspect is the quality of the ceramic TMB_2 target. Commercial targets sintered at high temperatures approaching 2000 °C often reach only around 80% of the theoretical density [17]. Therefore, the targets contain hidden porosity filled with contaminants (water vapor, oxygen, carbon, etc.). Since these elements can significantly influence the nucleation and growth of TMB_2 coatings, it is necessary to first pre-clean the target before deposition and then apply sufficiently high target power to reach a high proportion of sputtered species compared to impurities. Tengdelius et al. [53] reported an oxygen content of $3 \div 26$ at.% in highly oriented and epitaxial ZrB_2 coatings at target powers of 400 W and 100 W, respectively, which was manifested by an increase in electrical resistivity. However, it must be said that epitaxial growth requires specific conditions, such as high temperatures and slow film growth. In general, the presence of impurities on the growth and structure of TMB_2 coatings is not so dramatic and usually does not exceed 3 at. % if the chamber is sufficiently evacuated ($<10^{-3}$ Pa) and high target power densities are used [25, 36, 54].

The second aspect is the different angular distribution of sputtered atoms from the compound target. According to sputtering theory, the angular distribution of atoms should follow the cosine law. However, the sputtering of TMB_2 targets leads to inhomogeneous emission in terms of the spatial and energy distribution of sputtered atoms. Subsequent transport through the plasma further boosts these effects, resulting in discrepancies between the stoichiometry of the target and the TMB_2

coating. Significant deviations in the composition of coatings are usually observed in combinations of constituents with significant weight differences. Experimental results by Olson et al. [55] indicate that boron atoms are more easily emitted from the target after only a few collisions (primary knock-in mode). Due to the energy obtained from the directly incident ions, they scatter along the normal of the target. Conversely, heavier metal atoms are emitted by a classical collision cascade (secondary knock-in mode) and therefore scattered in a wide angular distribution [55]. This is in good agreement with, e.g., TiB_2 and ZrB_2 coatings, respectively, where the B/Ti (Zr) ratio often exceeds the value of 2 and the coatings are overstoichiometric. However, for TM diborides such as NbB_2 or TaB2, the B/Nb (Ta) ratio is usually much lower than 2, and the coatings are understoichiometric [54, 56, 57]. This is due to the third aspect—the resputtering of light boron from the growing coating. Resputtering is mainly the result of backscattered neutrals (neutralized gaseous Ar ions) from the target. Ar neutrals backscattered from heavy targets (TaB2) retain very high kinetic energy, which they transfer to knocking out large amounts of boron atoms from the coating. Resputtering is also a part of the deposition of lighter TM diborides such as TiB_2. But in this case, the kinetic energy of the reflected Ar neutrals is significantly lower, and the coatings still retain their overstoichiometric character [56].

All the mentioned aspects can be influenced by a suitable combination of deposition parameters (bias, substrate temperature, substrate-target distance, ion flux, target thickness, and others). This leads to the growth of TMB_2 coatings with the desired chemical composition and structure, as will be demonstrated in the following sections.

3.1 Compositional and Structural Evolution in Early Transition-Metal Diboride Coatings

The TiB_2 coating is an ideal representative for demonstrating differences in chemical composition due to the different angular distribution of sputtered species from a stoichiometric diboride compound target. The first important factor for observing differences in B/Ti is the location of the substrates relative to the normal axis of the magnetron. In cases where the substrate is located close to the intersection with the normal axis, TiB_2 are characterized by a large excess of boron and are overstoichiometric TiB_{2+z}, where $+z$ represents the excess of B ($TiB_{2.4}$ [25], $TiB_{2.7}$ [36], superstoichiometric $TiB_{4.42}$ [28], $TiB_{4.5}$ [58]). The more the surface of the substrate moves horizontally away from the normal axis, the more the amount of boron in TiB_2 coatings decreases, and the ratio approaches the stoichiometric ratio of 2 (Fuger et al. [28] reported the interval $2.07 \div 3.19$).

In general, the structure of the sputtered TiB_2 coatings is unique, having a nanocomposite character (see Fig. 4), where crystalline hexagonal a-TiB_2 nanocolumns (nanofilaments) with a diameter in the range of typically 5–20 nm nanometers are surrounded by an amorphous so-called B-tissue phase [25]. The
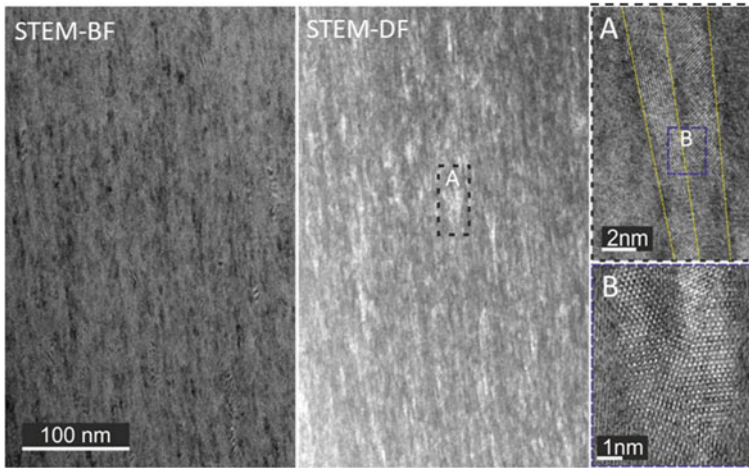
Fig. 4 Scanning transmission electron microscopy **a** bright-field (STEM-BF) and **b** dark-field (STEM-DF) cross-section image of as-deposited $TiB_{3.1}$ coating showing nanocolumnar character of the structure. **c** STEM-DF detail from region A showing interface between nanocolumns. **d** STEM-DF from region B showing detail of a very fine nanocolumns embedded in the disordered B-excess region

volume fraction of the tissue phase is given by the boron excess in the coating, and the increasing amount of the B-tissue phase suppresses the growth of crystalline TiB_2 nanocolumns (the diameter of the nanocolumns is close to ~3 ÷ 4 nm). However, the B/Ti ratio plays another important role from the point of view of structure, which is the preferential growth of crystalline planes of nanocolumns—texture. The preferential {0001} orientation is typical for slightly overstoichiometric TiB_2 coatings, but a change occurs at high boron contents when the {0001} texture is lost and the crystalline phase grows predominantly in the 10–11 direction [28, 36].

Significant differences in the stoichiometry of TiB_{2+z} coatings are reflected in the mechanical properties, especially in the hardness values. If the B/Ti ratio is in the range of about 2 to 3 and the {0001} texture dominates the coatings, the hardness of the coatings usually exceeds 40 GPa [25, 28, 36]. Here, the hardness is mainly achieved by the "ideal" size of the nanocolumns from the point of view of the Hall–Petch relation and the high cohesive strength between the very thin (thickness of a few atomic monolayers) B-tissue phase and the nanocolumns. The second reason for the superhardness is the intrinsic nature of the crystalline phase, given by strong covalent bonds. Finally, the high atomic density in the {0001} planes parallel to the substrate surface, acting very resistant to the diamond tip of the nanoindenter, also contributes significantly to the increase in hardness. In the case of superstoichiometric ratios B/Ti > 3, the hardness decreases significantly (even by tens of % [28]). This behavior is mainly due to excessive grain refinement (inverse Hall–Petch effect) and the loss of the 0001 preferential orientation. A large proportion of the soft B-tissue phase and

its decreasing cohesive strength also have a non-negligible effect on the decrease in hardness.

Magnetron sputtering is a highly variable technique, and the composition of TiB_2 coatings can be influenced by tuning of the tuneable deposition parameters. However, several of them are interconnected, and a change in one parameter can have a different effect on the growth of the TiB_2 coating when another parameter is simultaneously changed. The first deposition parameter is the pressure of the working (Ar) atmosphere—plasma. An increase in the pressure from the order of tenths of Pa to 1–2 Pa leads to a decrease in the B/Ti ratio from usually highly overstoichiometric toward ~2 [28, 59]. Increasing the pressure increases the plasma density, and light boron atoms are more scattered due to more frequent collisions with heavy Ar ions. On the other hand, for a given constant pressure, B/Ti increases with increasing distance (larger deposition angle) between target and substrate. In this case, the plasma density decreases with increasing distance from the target, and the collision-induced effects on the scattering of B atoms are weaker. It should be noted that the ionization energies of Ti and B atoms are lower compared to those of Ar atoms, meaning that their ionization in the plasma is easier. However, the number of Ar^+ ions found in the magnetron glow discharge is significantly higher than Ti^+ and B^+, respectively, due to their low sputtering yield. Therefore, the influence of ionized target species on the composition of TiB_2 coatings is negligible. The change of both deposition parameters, pressure and distance, affects the structure of the coatings, when the growth of the TiB_2 coating at higher pressures is accompanied by the formation of the {0001} texture and these coatings are harder. The 0001 highly oriented structure in TiB_2 coatings also dominates during depositions, when the target-substrate distance or the deposition angle, respectively, corresponds to the achievement of the B/Ti ratio <~3 [28].

Applying a negative substrate bias proved to be very important for the chemical and structural changes of TiB_2 coatings. In general, the bombardment of a growing film essentially causes atomic "peening", where the sputtered atoms localized on the surface are hit by heavy Ar ions and forced into voids and interstitial lattice spaces. This process leads to the densification of the material, reduction of grain size, and the generation of compressive macrostresses in the coating [60].

In the published results of Mikula et al., it was shown that increasing the bias voltage increases the kinetic energy of the incident Ar ions on the growing coating. This leads to a decrease in the B/Ti ratio due to the resputtering of boron atoms. But the implantation of a small amount of Ar ions (1–3 at.%) into the lattice was also observed. The resulting structure of such TiB_2 is typically nanocomposite, where the proportion of the 0001-oriented TiB_2 phase increases with the increasing energy of Ar ions. In addition, the coatings contain a number of point defects, which are manifested by high values of compressive macrostresses (σ ~ several GPa). The {0001} texture in combination with large macrostrains leads to an increase in hardness well exceeding ~40 GPa (~55 GPa [25], ~69 GPa [61] and ~73 GPa in the extremely strained TiB_2 coating [62]).

It is possible to suppress the negative effect of bias—the incorporation of Ar ions—by increasing the temperature of the substrates during deposition. TiB_2 coatings are highly temperature-stable, and their chemical composition and nanostructure practically do not change even at substrate temperatures of 700 °C [61, 62]. Argon begins to be released from the growing coating after exceeding the deposition temperature of 300 °C. The crystal lattice essentially behaves as relaxed, and the compressive macrostress values σ do not exceed 1 GPa. However, almost stress-free TiB_2 coatings still show extremely high hardness values exceeding 40 GPa due to their nanocomposite nature [61, 62].

The above results pointed out one important fact: magnetron-sputtered TiB_2 coatings are always overstoichiometric (B/Ti > 2) regardless of the combination of deposition parameters, and the nanostructure of TiB_2 coatings always contains a B-tissue phase. As will be shown in Sect. 4, the presence of the B-tissue phase plays a key role in the oxidation resistance or fracture toughness of diboride coatings, and its absence is often desirable. Petrov et al. [63] reported a way to achieve B/Ti ≈ 2 even in magnetron-sputtered TiB_2 coatings by amplifying the axial magnetic field using Helmholtz coils. In this way, the Ar plasma density increased, and the ionization of Ti atoms also improved (the number of Ti^+ ions increased). Subsequently, energetic Ti^+ ions were incorporated into the growing film and compensated for the quantitative difference between boron and titanium atoms [63].

ZrB_2 coatings also belong to the group of early transition-metal diboride coatings, which have received more attention. Tengdelius et al. reported several summary results in which they demonstrated the growth and structure of sputtered ZrB_2 coatings under different temperature conditions, such as no heating substrates up to a deposition temperature of 550 °C [64] or epitaxial growth on highly oriented substrates at temperatures reaching 900 °C [35, 53]. In the first case, the chemical composition of ZrB_2 coatings grown on Si (001) substrates in an industry-scaled device is close to stoichiometry B/Zr ≈ 2, especially at lower deposition temperatures [64]. The tendency toward a slight understoichiometry of B/Zr ~ 1.84 is associated with an increase in temperature to 550 °C. Despite worse vacuum conditions (high vacuum, HV) with a basic pressure of 10^{-3} Pa, typical for an industrial system, the amount of C and O_2 contaminants does not exceed 2 at.%. The microstructure of ZrB_2 coatings has a typical nanocolumnar character. Small differences in stoichiometry affected the preferential orientation of the coatings; while stoichiometric ZrB_2 grows preferentially in the 0001 direction, Zr-rich ZrB_{2-z} coatings are randomly oriented [64]. Ultra-high vacuum (UHV) conditions accompanied by a high deposition temperature (900 °C) together with the use of single-crystal 4H-SiC (0001) and Si (111) substrates enable the epitaxial growth of ZrB_2 coatings in the 0001 direction [65]. Decreasing the deposition temperature to 550 °C and sputtering power, respectively, leads to a change in the preferential orientation of nanocolumnar grains from 0001 to 10–11, which is mainly caused by the increasing concentration of impurities [53]. A detailed STEM study of epitaxially grown stoichiometric ZrB_2 coatings on Al_2O_3 (0001) at 900 °C shows a nanocomposite structure formed by ZrB_2 nanocolumns with a diameter of ~20 nm separated by a semi-coherent interface with a small B-excess [35]. In this context, the structures of slightly overstoichiometric

TiB_{2+z} and stoichiometric ZrB_2 coatings are the same. The ultrathin B-tissue phase increases the cohesive strength in the boundary region, which usually has the lowest resistance to distortion during nanoindentation. The hardness of 0001 epitaxially grown ZrB_2 is about 45 GPa, similar to TiB_{2+z} coatings [35].

3.2 Compositional and Structural Evolution in Late-Transition-Metal Diboride Coatings

Late-transition-metal diboride coatings well demonstrate the resputtering effect of the growing films. This becomes dominant during the reflection of Ar neutrals from the heavy compound target, resulting in the growth of understoichiometric TMB_{2-z} coatings, where -z means boron deficiency. As will be shown, the amount and localization of boron vacancies significantly affect the formation of the nanostructure and its mechanical properties. From the group of TMs (VB and VIB) diborides, TaB2 coatings represent a very promising alternative to TiB_2 and ZrB_2 coatings since tantalum itself is very interesting due to its temperature stability, oxidation resistance, and toughness. Grančič et al. [58] reported TaB2 coatings prepared by magnetron sputtering under standard deposition conditions that were highly substoichiometric B/Ta ~ 1.2, and transmission electron microscopy (TEM) investigation revealed the amorphous nature of their structure. Only the maximum reduction of the target voltage (~370 V), when the glow discharge was still working, reduced the kinetic energy of Ar neutrals reflected from the TaB2 target, which resulted in the growth of very fine nanocrystalline TaB1.7, but without the typical non-columnar character.

An extensive view of the compositional and structural changes of TaB2 coatings due to the change in the kinetic energy of Ar neutrals was reported in 2020 in the work of Šroba et al. [56]. Here, the experiments were performed using High Target Utilisation Sputtering (HiTUS) technology, where it is possible to independently change the kinetic energy of argon ions accelerated toward the target (target voltage control) while maintaining the same amount (constant target current). In this way, it was possible to vary the target voltage values from an extremely low 157 V to a very high 840 V. As can be seen from the elemental analysis results (Fig. 5a), TaB2 coatings grow in a wide composition ratio B/Ta from highly overstoichiometric TaB3.84 (157 V) to highly understoichiometric TaB1.36 (840 V).

To the explanation of resputtering effect, the involvement of energetic reflected Ar neutrals in sputtering from TaB2 target using incident Ar^+ ions was analyzed by simulation stopping and range of ions in matter (SRIM) software. The simulations assumed that the energy of incident Ar^+ ions on the target (in electron volts) was equal to the target potential (in volts) [56]. The output of this simulation is the energy distribution of reflected Ar neutrals at the substrate position (Fig. 5b). The percentage of reflected Ar neutrals above the target is approximately 14% with respect to the number of impinging Ar^+ ions. It was clearly seen that the number of reflected Ar
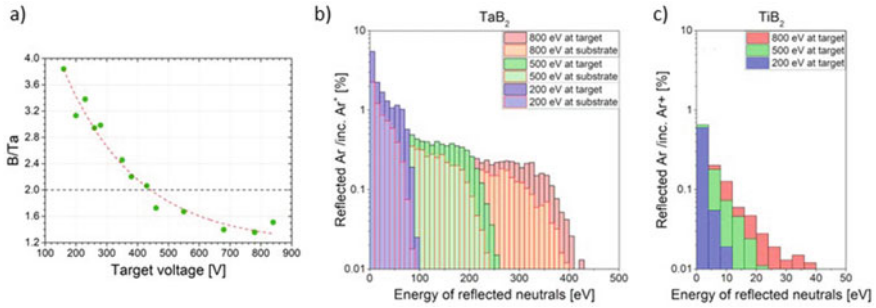
Fig. 5 **a** Boron-to-tantalum (B/Ta) ratio of films plotted as a function of target voltage. **b** Energy distribution of reflected Ar neutrals above TaB2 target position and at the substrate position (lighter color bars) for different energies of incident Ar$^+$. **c** Energy distribution of reflected Ar neutrals above the TiB$_2$ target [56]

neutrals at the substrate position is reduced compared to the target position (8%, 6%, and 4% for 200, 500, and 800 V, respectively); however, the shapes of energy distributions remain constant, and maximum values of energies are only slightly reduced, meaning that a significant number of highly energetic reflected Ar neutrals at substrate position can strongly affect the chemical composition of growing TaB2$_{\pm z}$ films, as was observed on magnetron sputtered TaB2$_{-z}$ films [58]. In comparison, the substantially smaller numbers, and values of energies of reflected neutrals were calculated for the well-known TiB$_2$ target (Fig. 5c). Here, the resputtering of boron is negligible typically leading to the formation of overstoichiometric TiB$_{2+z}$ films.

The wide compositional range is also reflected in the character of the structure of the growing TaB2 films. Essentially, all TaB2 coatings prepared by HiTUS are crystalline, consisting of a hexagonal α-TaB2 phase that forms a {0001} texture. However, this disappears at high boron contents, and the coatings have a rather randomly oriented polycrystalline character. A significant difference occurs when looking at the nanostructure of the coatings, as seen in Fig. 6a. The TaB3.84 coatings are nanocomposite with a very fine nanocolumnar TaB2 phase embedded in the B matrix (Fig. 6a). As the amount of boron in the almost stoichiometric TaB2.06 decreases, the in-plane size of the nanocolumns increases, and the volume fraction of the B-tissue phase decreases significantly (Fig. 6b). In highly substoichiometric TaB1.36 coatings, the B-tissue phase is absent, and the nanostructure is formed by large hexagonal crystalline areas (Fig. 6c). These regions contain numerous boron vacancies and Ta-rich stacking faults; however, interestingly, they are still able to retain their crystalline form. A certain explanation of the structural stability of TaB2 coatings with a high boron deficit is offered by the density functional theory (DFT) calculation of formation energies and density of states (DOS). As mentioned in Sect. 2, in TaB2, the Fermi level is not lying on the pseudogap but above the bottom of antibonding states, indicating that the number of valence electrons five also leads to filling the antibonding states and to a weakening of the chemical stability of TaB2. The introduction of boron vacancies moves E$_F$ toward the minimum of the
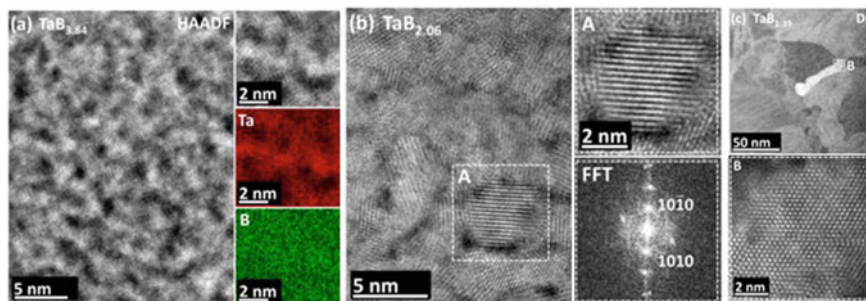
Fig. 6 a STEM-HAADF plane-view image of as-deposited highly overstoichiometric TaB3.84 film. The inset in (**a**) shows STEM-HAADF detail of a very fine-grained nanostructure with corresponding STEM-EDS maps of elemental distributions. **b** STEM-HAADF plane-view image of as-deposited TaB2.06 film showing the circle like outline of the nanocolumns (in the detail from region A is an individual nanocolumn with the size of a few nanometers) with the corresponding FFT pattern. **c** STEM-DF plane-view image of the as-deposited highly understoichiometric TaB1.39 film showing large nanocolumns formed by the α-TaB2 phase (atomic resolution image obtained from selected region B) [56]

pseudogap, which is an indication that $TaB2_{-z}$ is stabilized upon the formation of vacancies ($z > 1.625$) [56].

$TaB2_{\pm z}$ coatings are generally very hard, but hardness values vary depending on stoichiometry. First, the decisive factor determining the hardness is the volume fraction of the amorphous matrix, which is higher the lower the hardness value. In the case of TaB3.84 the hardness is 27 GPa. The highest hardness of 42 GPa achieved in TaB2.98 is the result of the optimal thickness of the B-tissue phase, where the cohesive force at the interface between the crystalline and amorphous phases is the highest. However, superhardness >40 GPa is preserved even in substoichiometric $TaB2_{-z}$ coatings. In these cases, the hardness is attributed to so-called vacancy-induced hardening. Namely, the presence of boron vacancies in the sublattice causes the strengthening of ion-covalent bonds between the neighboring boron and tantalum atoms, which may have a positive effect on hardness values [56].

Although HiTUS technology offers great possibilities in terms of the compositional and structural design of TaB2 coatings, it is not as widely used as conventional DC magnetron sputtering. Viskupová et al. [57] found the possibility of varying the B/Ta stoichiometry in a wider concentration range from 1.3 to 2, even during deposition by magnetron sputtering. Here, the decrease of target thickness from 6 to 4 mm and accompanied increase of permanent magnetic field above the target surface influences the plasma density and the target voltage (decrease from ~460 to ~260 V) corresponding to specific target current. This way the energy distribution of Ar neutrals shifts to smaller energies, which ultimately leads to the reduced resputtering of light boron from the coating and thus increased the B/Ta ratio toward 2.

An additional method that affects the B/Ta ratio is the application of an external magnetic field using Helmholtz coils. This causes an increase in the plasma density

near the substrates and leads to the preferential ionization of Ta atoms and consequently to the reduction of the B/Ta ratio. Stoichiometric TaB2 was crystalline, containing the 0001-oriented α-TaB2 phase. The reduction of B/Ta from 2 to 1.8 was accompanied by a change in the preferred orientation from 0001 to 10–11. A further decrease of B/Ta toward 1.3 led to the formation of an almost X-ray amorphous structure. The hardness of the TaB2 coatings agreed with the structure, when the highest hardness of 48 GPa was shown by the almost stoichiometric, highly oriented TaB1.91 coatings. On the contrary, the hardness of highly substoichiometric, almost amorphous coatings reached about 31 GPa [57].

An important fact emerges from this study: since the energy of Ar neutrals is influenced by the thickness of the target, its gradual erosion changes the B/Ta ratio. This can affect the reproducibility of the coating properties during long-term use of the target. Therefore, the lifetime of the target must be estimated by regular inspection of test samples.

Several works also pay attention to other transition-metal (VB and VIB) diboride coatings, such as NbB_2, MoB_2, and WB_2, where their growth is accompanied by a significant resputtering effect [54, 66, 67]. As discussed in Sect. 2, the chemical stability of the α-type structure of late TM diborides is reduced due to the occupation of antibonding states by excess valence electrons. However, the formation of vacancies in the boron sublattice reduces the number of states near the Fermi level and strengthens the TM–B interactions, leading to a chemical stabilization of the α-type structure [68]. This fact is in good agreement with the following experimental results, where a slight deficit of boron in the coatings does not lead to the collapse of the hexagonal lattice.

Nedfors et al. [54] reported the structural evolution of understoichiometric $NbB_{1.8}$ coatings sputtered from a stoichiometric NbB_2 target. Despite the slight boron deficiency, the coatings were crystalline, formed by the α-NbB_2 phase, with a weak {0001} texture. A deeper look into the nanostructure revealed the presence of a self-organized nanocomposite formed by vacancies containing NbB_{2-z} nanocolumns surrounded by a very thin B-tissue phase. As in the TaB_{2-z} coatings, the NbB_{2-z} coatings are superhard due to vacancy-induced hardening, when the hardness of the $NbB_{1.8}$ coating reaches 42 GPa.

Similar behavior was also observed in the case of MoB_{2-z} coatings obtained by sputtering a stoichiometric MoB_2 target [66]. The understoichiometric $MoB_{1.6}$ coatings had a dense columnar character consisting of MoB_{2-z} nanocolumns with a diameter of several nanometers surrounded by a B-tissue phase. Nanoindentation measurements revealed a relatively high hardness of 29 GPa.

The α-AlB_2-type structure stabilized by boron vacancies was also observed in sputtered WB_{2-z} coatings [67]. The hardness of WB_{2-z} coatings was significantly influenced by the preferential orientation of the nanocolumns. Purely 0001-oriented $WB_{1.87}$ coatings achieved a superhardness of 40 GPa; however, texture suppression and concurrent growth of nanocolumns in the 0001 as well as 10–11 directions occurred during the deposition of $WB_{1.55}$ coatings led to a significant decrease in hardness to 25 GPa.